10-5-2011

Theoretical Analysis of Quantum Ghost Imaging Through Turbulence

Kam Wai Clifford Chan
Rochester Optical Manufacturing Company

D. S. Simon
Boston University

A. V. Sergienko
Boston University

Nicholas D. Hardy
Massachusetts Institute of Technology

Jeffrey H. Shapiro
Massachusetts Institute of Technology

See next page for additional authors

Recommended Citation

K. W. C. Chan, DS Simon, A. V. Sergienko, N. D. Hardy, J. H. Shapiro, and P. B. Dixon, *Theoretical Analysis of Quantum Ghost Imaging Through Turbulence*, Phys. Rev. A **84**(4), 043807. https://doi.org/10.1103/PhysRevA.84.043807

Theoretical Analysis of Quantum Ghost Imaging Through Turbulence

Authors

Kam Wai Clifford Chan, D. S. Simon, A. V. Sergienko, Nicholas D. Hardy, Jeffrey H. Shapiro, P. Ben Dixon, Gregory A. Howland, John C. Howell, Joseph H. Eberly, Malcolm N. O'Sullivan, Brandon Rodenburg, and Robert W. Boyd

Theoretical analysis of quantum ghost imaging through turbulence

Kam Wai Clifford Chan,[1] D. S. Simon,[2] A. V. Sergienko,[2] Nicholas D. Hardy,[3] Jeffrey H. Shapiro,[3] P. Ben Dixon,[4] Gregory A. Howland,[4] John C. Howell,[4] Joseph H. Eberly,[4] Malcolm N. O'Sullivan,[5] Brandon Rodenburg,[5] and Robert W. Boyd[4,5,6]

[1]*Rochester Optical Manufacturing Company, 1260 Lyell Avenue, Rochester, New York 14606, USA*

[2]*Department of Electrical and Computer Engineering, Boston University, Boston, Massachusetts 02215, USA*

[3]*Research Laboratory of Electronics, Massachusetts Institute of Technology, 77 Massachusetts Avenue, Cambridge, Massachusetts 02139, USA*

[4]*Department of Physics and Astronomy, University of Rochester, Rochester, New York 14627, USA*

[5]*Institute of Optics, University of Rochester, Rochester, New York 14627, USA*

[6]*Department of Physics, University of Ottawa, Ottawa, Ontario K1N 6N5, Canada*

(Received 12 July 2011; published 5 October 2011)

Atmospheric turbulence generally affects the resolution and visibility of an image in long-distance imaging. In a recent quantum ghost imaging experiment [P. B. Dixon *et al.*, Phys. Rev. A **83**, 051803 (2011)], it was found that the effect of the turbulence can nevertheless be mitigated under certain conditions. This paper gives a detailed theoretical analysis to the setup and results reported in the experiment. Entangled photons with a finite correlation area and a turbulence model beyond the phase screen approximation are considered.

DOI: 10.1103/PhysRevA.84.043807 PACS number(s): 42.30.Va, 42.68.Bz, 03.67.Hk

I. INTRODUCTION

Ghost imaging (GI) is a procedure for forming the image of an object indirectly by means of correlation measurements. The topic was originally developed to demonstrate the unusual nonlocal effect of entangled photons [1], first observed as two-photon ghost interference and diffraction [2,3]. In the context of imaging, it has been demonstrated that GI can be obtained by using entangled photons produced by spontaneous parametric down-conversion (SPDC) [4] or thermal light [5,6]. The setups of the two cases are similar. Here we focus on the quantum case using entangled photons.

In a GI setup, one of the photons (the signal photon) is sent to illuminate an object. The photons transmitted are captured by a detector (the object detector) that does not need to have spatial resolution. On the other hand, the other photon (the idler photon) is registered by a detector (the reference detector) that has spatial resolution capability. An image (the ghost image) is formed by coincidence measurements between the object and the reference detectors.

GI is so-called because the photons that provide the spatial information regarding the object have never directly interacted with the object to be imaged. The distributed nature of GI thus makes it a clear candidate in distributed image processing, as well as in distributed sensing and communication schemes. In such applications, imaging through turbulence becomes unavoidable. The effect of turbulence on GI performance has begun to be investigated theoretically [7–9]. These analyses show that the quality of the ghost image decreases as the strength of the turbulence increases. Experiments using thermal light and entangled photons have also been performed recently [10,11] and interesting results have been obtained. In particular, Dixon *et al.* [11] demonstrated that a certain degree of the turbulent effect on the ghost image can be mitigated under suitable conditions.

In this paper, we give a detailed theoretical analysis to the experiment in Ref. [11]. The entangled photons are taken to have a finite correlation area. We consider both the phase screen model as well as the finite-thickness model for the turbulent medium.

II. QUANTUM GI SYSTEM THROUGH A TURBULENT MEDIUM

In the calculation below, we take the measurement time of the detectors to be much longer than the variation time scale of the turbulent medium, which is of the order of 10 ms. In this way, a statistical average over the phase distortion imposed by the turbulent medium is made. In addition, the temporal behavior of the ghost image is suppressed for simplicity.

A typical quantum GI configuration with a turbulent medium is depicted in Fig. 1(a). We assume that the photons transmitted by the object are all collected by the object detector so that the detector can be taken to be in the immediate vicinity of the object. The ghost image is given by [4]

$$P(\vec{x}_r) = \int d\vec{x}_o |T(\vec{x}_o)|^2 G^{(2)}(\vec{x}_o,\vec{x}_r), \tag{1}$$

where $T(\vec{x})$ is the object's field transmission function and

$$G^{(2)}(\vec{x}_o,\vec{x}_r) = \langle \mathrm{Tr}[\rho \hat{E}_r^{(-)}(\vec{x}_r)\hat{E}_o^{(-)}(\vec{x}_o)\hat{E}_o^{(+)}(\vec{x}_o)\hat{E}_r^{(+)}(\vec{x}_r)]\rangle \tag{2}$$

is the second-order coherence function at the detector planes. Here $\langle\cdots\rangle$ is the statistical ensemble average due to the turbulence motion. Note that, because of the presence of the turbulent medium, the quantum state is no longer a pure state in the detector planes.

It is useful to write the second-order coherence function in terms of that in the source planes:

$$\begin{aligned} G^{(2)}(\vec{x}_o,\vec{x}_r) = &\int d\vec{x}_i' \int d\vec{x}_s' \int d\vec{x}_s \int d\vec{x}_i \\ &\times \langle H_r^*(\vec{x}_r,\vec{x}_i') H_o^*(\vec{x}_o,\vec{x}_s') H_o(\vec{x}_o,\vec{x}_s) H_r(\vec{x}_r,\vec{x}_i)\rangle \\ &\times \mathrm{Tr}[\rho \hat{E}_i^{(-)}(\vec{x}_i')\hat{E}_s^{(-)}(\vec{x}_s')\hat{E}_s^{(+)}(\vec{x}_s)\hat{E}_i^{(+)}(\vec{x}_i)]. \end{aligned} \tag{3}$$

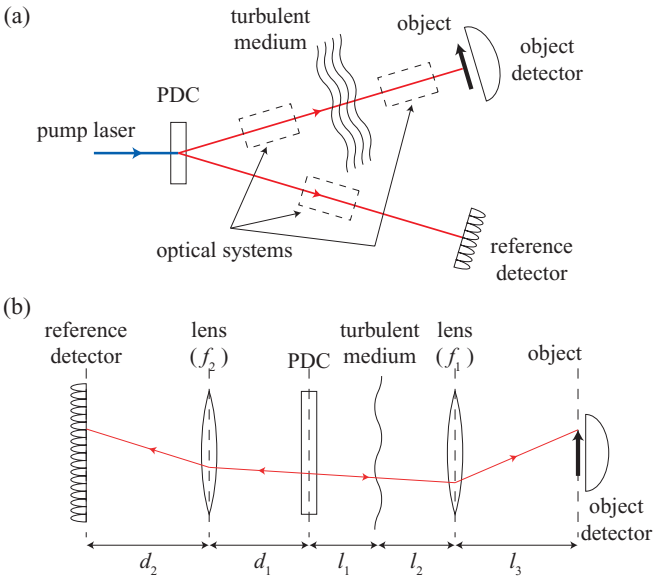

FIG. 1. (Color online) (a) A generic quantum GI setup with a turbulent medium inserted in the object arm. (b) The Klyshko picture of a model setup for the theoretical description in this paper.

$H_o(\vec{x}_o,\vec{x}_s)$ and $H_r(\vec{x}_r,\vec{x}_i)$ are the propagators of the object and reference arms, respectively. The subscripts o and r denote object and reference photons and s and i denote the signal and idler photons. The signal photon is used for object illumination while the idler photon is used as the reference beam. To proceed, we need to specify the details of the optical systems in the object and reference arms. We consider the double-lens configuration shown in Fig. 1(b), which is drawn in the unfolded form (the Klyshko picture) [1,2,4]. Different locations of the turbulent medium are considered later in Sec. IV.

According to Fig. 1(b), The reference arm propagator is given by

$$H_r(\vec{x}_r,\vec{x}_i) = \int d\vec{\xi}_r\; h_{d_2}(\vec{x}_r,\vec{\xi}_r) L_{f_2}(\vec{\xi}) h_{d_1}(\vec{\xi}_r,\vec{x}_i), \tag{4}$$

where

$$h_d(\vec{x},\vec{\xi}) = \frac{k e^{ikd}}{2\pi i d} \exp\left[\frac{ik}{2d}|\vec{x}-\vec{\xi}|^2\right] \tag{5}$$

is the free-space propagator, and $L_f(\vec{x})$ is the quadratic phase factor by a lens of focal length f. We assume that the lenses are infinitely large (i.e., much larger than the transverse beam size of the signal and idler beams) in calculating the propagators H_o and H_r. Note that $\lim_{d\to 0} h_d(\vec{x},\vec{\xi}) = \delta(\vec{x}-\vec{\xi})$. On the other hand, the object arm propagator is

$$H_o(\vec{x}_o,\vec{x}_s) = \int d\vec{\xi}_o \int d\vec{\eta}_o \int d\vec{\zeta}_o\; h_{l_3}(\vec{x}_o,\vec{\zeta}_o) L_{f_2}(\vec{\zeta}_o) \times h_{l_2}(\vec{\zeta}_o,\vec{\eta}_o) h_{\rm turb}(\vec{\eta}_o,\vec{\xi}_o) h_{l_1}(\vec{\xi}_o,\vec{x}_s), \tag{6}$$

where $h_{\rm turb}(\vec{\eta}_o,\vec{\xi}_o)$ is the propagator in the turbulent medium, which is given explicitly in the next section. Substituting Eq. (5) into Eqs. (4) and (6), we obtain

$$H_r(\vec{x}_r,\vec{x}_i) = \frac{k e^{ik(d_1+d_2)}}{2\pi i\delta} \exp\left[\frac{ik}{2\delta}|\vec{x}_r-\vec{x}_i|^2\right] \times \exp\left[-\frac{ik}{2\delta f_2}(d_1|\vec{x}_r|^2 + d_2|\vec{x}_i|^2)\right] \tag{7}$$

and

$$H_o(\vec{x}_o,\vec{x}_s) = \frac{k e^{ik(l_2+l_3)}}{2\pi i\ell} \int d\vec{\eta}_o \exp\left[\frac{ik}{2\ell}|\vec{x}_o-\vec{\eta}_o|^2\right] \times \exp\left[-\frac{ik}{2\ell f_1}(l_2|\vec{x}_o|^2 + l_3|\vec{\eta}_o|^2)\right] H_{\rm turb}(\vec{\eta}_o,\vec{x}_s), \tag{8}$$

where $\delta = (d_1+d_2) - d_1 d_2/f_2$, $\ell = (l_2+l_3) - l_2 l_3/f_1$, and

$$H_{\rm turb}(\vec{\eta}_o,\vec{x}_s) = \frac{k e^{ikl_1}}{2\pi i l_1} \int d\vec{\xi}_o\; h_{\rm turb}(\vec{\eta}_o,\vec{\xi}_o) \exp\left[\frac{ik}{2l_1}|\vec{\xi}_o-\vec{x}_s|^2\right]. \tag{9}$$

III. MODEL FOR THE TURBULENCE MEDIUM

To obtain the second-order coherence function, we need to calculate the ensemble average:

$$\langle H_{\rm turb}(\vec{\eta}_o,\vec{x}_s) H^*_{\rm turb}(\vec{\eta}'_o,\vec{x}'_s)\rangle = \frac{k^2}{(2\pi)^2 l_1^2} \int d\vec{\xi}_o \int d\vec{\xi}'_o\; \langle h_{\rm turb}(\vec{\eta}_o,\vec{\xi}_o) h^*_{\rm turb}(\vec{\eta}'_o,\vec{\xi}'_o)\rangle \times \exp\left[\frac{ik}{2l_1}(|\vec{\xi}_o-\vec{x}_s|^2 - |\vec{\xi}'_o-\vec{x}'_s|^2)\right]. \tag{10}$$

Utilizing the extended Huygens-Fresnel principle in the paraxial approximation, the turbulence propagator for a medium of thickness L is given by

$$h_{\rm turb}(\vec{\eta}_o,\vec{\xi}_o) = \frac{k e^{ikL}}{2\pi i L} \exp\left[\frac{ik}{2L}|\vec{\eta}_o-\vec{\xi}_o|^2 + \psi(\vec{\eta}_o,\vec{\xi}_o)\right], \tag{11}$$

where the complex phase $\psi(\vec{\eta}_o,\vec{\xi}_o)$ has real and imaginary parts that represent, respectively, the turbulence-induced log-amplitude and phase fluctuations imposed on a spherical wave propagating from $(\vec{\xi}_o,0)$ to $(\vec{\eta}_o,L)$. The mutual coherence function of the propagation kernel $h_{\rm turb}(\vec{\eta}_o,\vec{\xi}_o)$ is given by [12]

$$\begin{aligned}\langle h_{\rm turb}(\vec{\eta}_o,\vec{\xi}_o) h^*_{\rm turb}(\vec{\eta}'_o,\vec{\xi}'_o)\rangle &= \frac{k^2}{(2\pi)^2 L^2} \exp\left[\frac{ik}{2L}|\vec{\eta}_o-\vec{\xi}_o|^2 - \frac{ik}{2L}|\vec{\eta}'_o-\vec{\xi}'_o|^2\right] \times \langle \exp[\psi(\vec{\eta}_o,\vec{\xi}_o) + \psi^*(\vec{\eta}'_o,\vec{\xi}'_o)]\rangle \\ &= \frac{k^2}{(2\pi)^2 L^2} \exp\left[\frac{ik}{2L}|\vec{\eta}_o-\vec{\xi}_o|^2 - \frac{ik}{2L}|\vec{\eta}'_o-\vec{\xi}'_o|^2\right] \times \exp\left[-\frac{1}{2}D_\psi(\vec{\xi}_o-\vec{\xi}'_o,\vec{\eta}_o-\vec{\eta}'_o)\right],\end{aligned} \tag{12}$$

where

$$D_\psi(\vec{\xi}_o-\vec{\xi}'_o,\vec{\eta}_o-\vec{\eta}'_o) = 2.91 k^2 L \int_0^1 ds\; C_n^2(sL) \times |s(\vec{\eta}_o-\vec{\eta}'_o) + (1-s)(\vec{\xi}_o-\vec{\xi}'_o)|^{5/3}, \tag{13}$$

with $C_n^2(z)$ being the refractive index structure constant. Note that Eq. (12) is applicable to the weak turbulence regime that follows the Kolmogorov spectrum, as well as deep into the regime of saturated scintillation [12]. Because of the fractional power in Eq. (13), numerical computation is required in order to proceed further. Here we take the quadratic approximation to obtain an analytic expression [13]. This approximation only imposes small modifications to the form and value of the mutual coherence function. Under the quadratic approximation and assuming a uniform C_n^2 profile, we have

$$\exp\left[-\tfrac{1}{2}D_\psi(\vec{\xi}_o-\vec{\xi}_o',\vec{\eta}_o-\vec{\eta}_o')\right] \approx e^{-\frac{1}{2\rho_0^2}[|\vec{\xi}_o-\vec{\xi}_o'|^2+(\vec{\xi}_o-\vec{\xi}_o')\cdot(\vec{\eta}_o-\vec{\eta}_o')+|\vec{\eta}_o-\vec{\eta}_o'|^2]}, \tag{14}$$

where $\rho_0=(1.09k^2C_n^2L)^{-3/5}$ is the coherence length of a spherical wave propagating in the turbulent medium.

We first consider the situation when the free-space propagation distances are much larger than the propagation distance in the turbulent medium (the phase screen approximation), which is valid for the experimental conditions of Ref. [11]. A finite-thickness model for the turbulent medium is considered later in Sec. V. Under the phase screen approximation, we further take $L\to 0$ so that

$$\langle h_{\rm turb}(\vec{\eta}_o,\vec{\xi}_o)h_{\rm turb}^*(\vec{\eta}_o',\vec{\xi}_o')\rangle \to \delta(\vec{\eta}_o-\vec{\xi}_o)\delta(\vec{\eta}_o'-\vec{\xi}_o')\exp\left[-\frac{\alpha}{2}|\vec{\xi}_o-\vec{\xi}_o'|^2\right], \tag{15}$$

where $\alpha=3/\rho_0^2$. As a result,

$$\langle H_{\rm turb}(\vec{\eta}_o,\vec{x}_s)H_{\rm turb}^*(\vec{\eta}_o',\vec{x}_s')\rangle = \frac{k^2}{(2\pi)^2l_1^2}\exp\left[-\frac{\alpha}{2}|\vec{\eta}_o-\vec{\eta}_o'|^2\right] \times\exp\left[\frac{ik}{2l_1}(|\vec{\eta}_o-\vec{x}_s|^2-|\vec{\eta}_o'-\vec{x}_s'|^2)\right]. \tag{16}$$

Using Eqs. (8) and (16), we obtain

$$\begin{aligned}\langle H_o(\vec{x}_o,\vec{x}_s)H_o^*(\vec{x}_o',\vec{x}_s')\rangle &= \frac{k^2}{(2\pi)^2\ell'^2}\exp\left[\frac{ik}{2\ell'}(|\vec{x}_o-\vec{x}_s|^2-|\vec{x}_o'-\vec{x}_s'|^2)\right]\\ &\times\exp\left\{-\frac{ik}{2\ell' f_1}[(l_1+l_2)\left(|\vec{x}_o|^2-|\vec{x}_o'|^2\right)\right.\\ &\left.+l_3(|\vec{x}_s|^2-|\vec{x}_s'|^2)]\right\}\exp\left[-\frac{\alpha}{2\ell'^2}|l_1(\vec{x}_o-\vec{x}_o')\right.\\ &\left.+\ell(\vec{x}_s-\vec{x}_s')|^2\right],\end{aligned} \tag{17}$$

where $\ell'=(l_1+l_2+l_3)-(l_1+l_2)l_3/f_1$. It is noted that some interesting observations can be seen directly from Eq. (17). When $\vec{x}_o=\vec{x}_o'$, the exponent with α vanishes when $\ell=0$. On the other hand, when $\vec{x}_s=\vec{x}_s'$, the same term vanishes only when $l_1=0$. We give physical interpretations to these two scenarios in the next section.

IV. RESOLUTION AND VISIBILITY OF THE GHOST IMAGE

In this section, the resolution and the visibility of the quantum ghost image are determined analytically. The turbulent layer can be located in various positions of the GI system, and we consider the four configurations depicted in Fig. 2. It is shown below that one can obtain the results of the other three configurations by using that of configuration 1 with proper reparametrization of the distances of the setup.

For configuration 1, we have

$$l_1=z,\quad l_2=2f+\Delta-z,\quad l_3=2f,$$
$$d_1=2f-\Delta,\quad d_2=2f,\quad f_1=f_2=f. \tag{18}$$

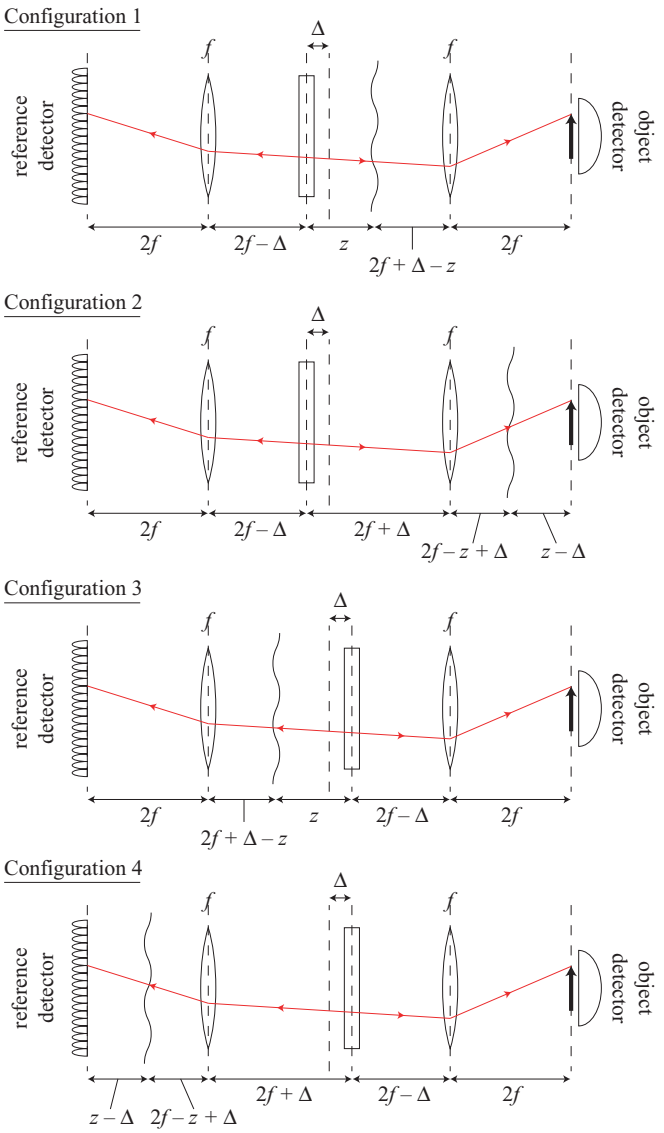

FIG. 2. (Color online) The experimental configurations considered in Dixon *et al.* [11]. In configurations 1 and 2, the turbulent layer (phase screen) is located in the object arm. In configurations 3 and 4, the layer is located in the reference arms. The distances l_i and d_j and the focal lengths of the lenses are chosen such that the four configurations give similar results (see the text).

As a result, the second-order coherence function is found to be

$$\begin{aligned} G^{(2)}(\vec{x}_o,\vec{x}_r) &= \frac{k^4}{(2\pi)^4\Delta^4}\int d\vec{x}_i' \int d\vec{x}_s' \int d\vec{x}_s \int d\vec{x}_i \\ &\times \exp\left[-\frac{ik}{2\Delta}\left(|\vec{x}_i|^2-|\vec{x}_i'|^2\right)\right]\exp\left[-\frac{ik}{\Delta}\vec{x}_r\cdot(\vec{x}_i-\vec{x}_i')\right] \\ &\times \exp\left[-\frac{\alpha}{2}\left(\frac{\Delta-z}{\Delta}\right)^2|\vec{x}_s-\vec{x}_s'|^2\right] \\ &\times \exp\left[\frac{ik}{2\Delta}(|\vec{x}_s|^2-|\vec{x}_s'|^2)\right]\exp\left[\frac{ik}{\Delta}\vec{x}_o\cdot(\vec{x}_s-\vec{x}_s')\right] \\ &\times \Psi(\vec{x}_s,\vec{x}_i)\Psi^*(\vec{x}_s',\vec{x}_i'), \end{aligned} \tag{19}$$

where $\Psi(\vec{x}_s,\vec{x}_i)$ is the biphoton wave function generated by the SPDC process. In general, the wave function exhibits rich spatial correlation features [14]. We consider the simplest case of the collinear type II SPDC process, in which $\Psi(\vec{x}_s,\vec{x}_i)$ can be approximated by the double-Gaussian model [15]

$$\Psi(\vec{x}_s,\vec{x}_i) = \frac{\sqrt{AB}}{\pi}e^{-\frac{A}{4}|\vec{x}_s+\vec{x}_i|^2}e^{-\frac{B}{4}|\vec{x}_s-\vec{x}_i|^2}, \tag{20}$$

with $A>0$ and $B>0$, which are related to the beam radius and transverse correlation distance through

$$a_0 = \frac{1}{2}\sqrt{\frac{1}{A}+\frac{1}{B}}, \quad \rho_c = \frac{1}{\sqrt{A+B}}. \tag{21}$$

In this way, the ghost image is found to be

$$\begin{aligned} P(\vec{x}_r) &= \frac{1}{(2\pi W_{\rm FOV}W_{\rm PSF})^2}\exp\left(-\frac{|\vec{x}_r|^2}{2W_{\rm FOV}^2}\right) \\ &\times \int d\vec{x}_o\,|T(\vec{x}_o)|^2\exp\left(-\frac{|\vec{x}_o+m\vec{x}_r|^2}{2W_{\rm PSF}^2}\right), \end{aligned} \tag{22}$$

where

$$W_{\rm FOV} = \sqrt{a_0^2+\frac{\Delta^2}{4k^2\rho_c^2}} \tag{23}$$

is the field of view,

$$W_{\rm PSF} = \left[\left(\rho_c^2+\frac{\Delta^2}{4k^2a_0^2}\right)+\frac{\alpha(\Delta-z)^2}{k^2}\right]^{1/2} \tag{24}$$

is the width of the point spread function, and

$$m = \pm\sqrt{1-\frac{\rho_c^2}{a_0^2}} \tag{25}$$

is the correlation factor, with plus (minus) sign for $A>B$ ($A<B$). Note that this correlation factor is purely due to the spatial correlation of the two entangled photons and is to be distinguished from the magnification of the optical system, which has unity magnification. Also it is remarked that the forms of $W_{\rm FOV}$ and the first term of $W_{\rm PSF}$ exhibit the widths of a diffracted Gaussian beam propagated for a distance of Δ.

From the expressions of $W_{\rm FOV}$, $W_{\rm PSF}$, and m, we see that, under the quadratic phase screen approximation to the turbulent layer, the turbulence only degrades the resolution of the ghost image; it has no effect on the field of view. As expected, no ghost image is formed when $a_0=\rho_c$, or equivalently $A=B$, i.e., the object and reference photons are disentangled. An interesting point to note is that the turbulence never totally destroys the correlation between the object and the reference photons (m is independent of α), even though the entanglement between them can vanish [16]. Nevertheless, $W_{\rm PSF}$ can become larger than the spatial feature of the object such that the ghost image is totally blurred.

As already noted from Eq. (17), the turbulence is compensated when $z=\Delta$. This has the same effect as bringing the object to the plane of the turbulent layer (or equivalently locating the turbulent layer in the central image plane) and hence the turbulence does not blur out the feature of the object.

For configuration 2, the calculations are identical to those of configuration 1, except that the roles of $\vec{x}_o$ ($\vec{x}_o'$) and $\vec{x}_s$ ($\vec{x}_s'$) in Eq. (17) are interchanged. By setting

$$\begin{aligned} l_1 = 2f+\Delta, \quad l_2 = 2f+\Delta-z, \quad l_3 = z-\Delta, \\ d_1 = 2f-\Delta, \quad d_2 = 2f, \quad f_1 = f_2 = f, \end{aligned} \tag{26}$$

it can be shown that the second-order coherence function is identical to that of the first configuration. The paremeters in Eq. (26) can be obtained by noting that, to keep Eq. (17) invariant, l_1+l_2 in configuration 2 should take the value of $l_3=2f$ as in configuration 1, and l_1 should take the value $\ell=z-\Delta$, while keeping ℓ', f_1, f_2, d_1, and d_2 the same as in configuration 1. As a result, the ghost image for configuration 2 is also given by Eqs. (22) to (25). The condition to mitigate the turbulence effect now is $z=\Delta$, i.e., the turbulence phase screen is on the real object plane instead of on the effective object plane as in configuration 1.

The representative ghost images of Ref. [11] fitted with Eq. (22) are shown in Fig. 3. The object is a one-dimensional test pattern of five slits defined by

$$T(x) = \sum_{n=-2}^{2}\theta\left(\frac{1}{2}-\left(\frac{x}{d}-2n\right)\right)\theta\left(\left(\frac{x}{d}-2n\right)+\frac{1}{2}\right), \tag{27}$$

where $\theta(x)$ is the step function. Using the single count data of the reference detector with $\Delta=0$ [the envelope function of Eq. (22)], the beam width is found to be $W_{\rm FOV}|_{\Delta=0}=a_0=0.362\pm0.006$ mm. The correlation distance is obtained from the ghost images with $\Delta=0$, which is $W_{\rm PSF}|_{\Delta=0}=\rho_c=0.019\pm0.003$ mm. The correlation factor is thus given by $m\approx1.00$, which is consistent with the observed images. The fitted slit width is $d=0.124\pm0.007$ mm, which is smaller than the given value of 0.139 mm in Ref. [11]. This discrepancy may be due to the object being tilted with respect to the object beam. Finally, the turbulence parameter is determined to be $\alpha=4.0\pm1.3$ mm^{-2}, which differs from that reported in Ref. [11] because of the different theoretical model used.

The visibility is defined as

$$V = \frac{P(0)-P(d)}{P(0)+P(d)}, \tag{28}$$

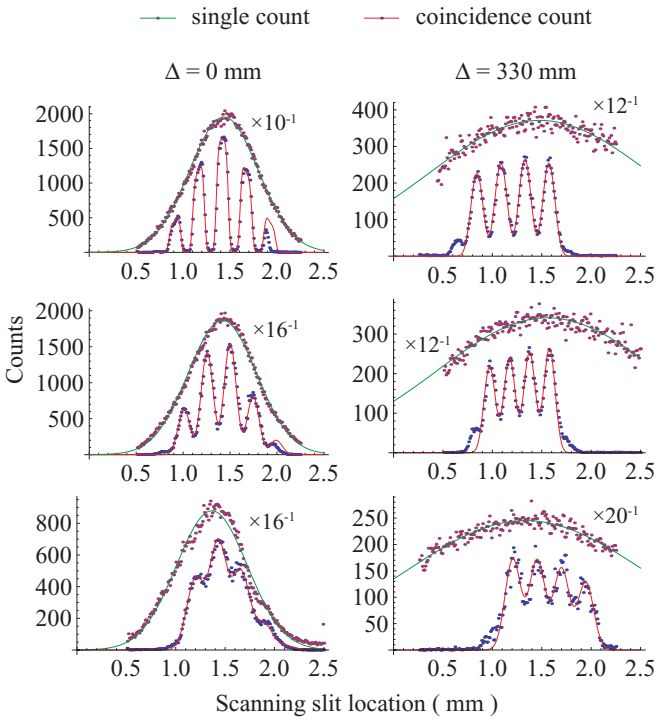

FIG. 3. (Color online) Representative ghost images (cf. Ref. [11]) with theoretical fits using Eq. (22) and object transmission function (27). The left and the right columns represent the unshifted ($\Delta = 0$) and the shifted ($\Delta = 330$ mm) configurations, respectively. Note that the unshifted data (left) are fitted with an object of five slits whereas the shifted data (right) are fitted with an object of four slits. The top row shows images with no turbulence. The middle row shows images for turbulence between the lens and the object, 203 mm (right) and 229 mm (left) from the object. The bottom row shows images for turbulence between the crystal and the lens, 483 mm (right) and 432 mm (left) from the crystal. Shown also are the single counts of the reference detector [the envelope function of Eq. (22)] scaled by the factors adjacent to the plots.

with $W_{\rm FOV}$ set to infinity. Using Eqs. (22) and (27), and under the conditions of the experiment, we obtain

$$V \approx 1 - \sum_{n=-2}^{2} \left[\mathrm{Erf}\left(\frac{(4n+3)d}{2\sqrt{2}W_{\rm PSF}}\right) - \mathrm{Erf}\left(\frac{(4n+1)d}{2\sqrt{2}W_{\rm PSF}}\right)\right], \tag{29}$$

where $\mathrm{Erf}(x)$ is the error function. As expected, the visibility is governed by the ratio of the slit width d and the width of the point spread function $W_{\rm PSF}$. The visibilities of the ghost image for configurations 1 and 2 as functions of the location of the turbulent medium are plotted in Fig. 4. It can be noted that the data plotted in Fig. 4(b) do not agree with the theoretical curves as well as the data plotted in Fig. 4(a). The reason is that, in that setup, the turbulence source—an 800° heat gun—was located fairly close to the nonlinear crystal. This could effectively have temperature-tuned the crystal away from correct alignment, resulting in a slightly different quantum state. Hence the fitting of the theory to the experimental data is poorer.

The situation when the turbulent layer is located in the reference arm instead of in the object arm (see configurations 3 and 4 in Fig. 2) can be analyzed easily. This is done by noting that the second-order coherence function in Eq. (19) does not distinguish between the object or reference arms other than the labeling of the variables. In addition, the biphoton wave function (20) is also symmetric in the signal and idler photons. The ghost image is thus obtained from Eq. (22) by interchanging $\vec{x}_o$ and $\vec{x}_r$ and is given by

$$\begin{aligned} P(\vec{x}_r) &= \frac{1}{(\pi W_{\rm FOV} W_{\rm PSF})^2} \int d\vec{x}_o \, |T(\vec{x}_o)|^2 \\ &\quad \times \exp\left(-\frac{|\vec{x}_o|^2}{2W_{\rm FOV}^2}\right) \exp\left(-\frac{|\vec{x}_r + m\vec{x}_o|^2}{2W_{\rm PSF}^2}\right) \\ &= \frac{1}{(\pi W_{\rm FOV} W_{\rm PSF})^2} \exp\left(-\frac{\beta|\vec{x}_r|^2}{2W_{\rm FOV}^2}\right) \\ &\quad \times \int d\vec{x}_o \, |T(\vec{x}_o)|^2 \exp\left(-\frac{|\vec{x}_r + \beta m\vec{x}_o|^2}{2\beta W_{\rm PSF}^2}\right), \end{aligned} \tag{30}$$

where $W_{\rm FOV}$, $W_{\rm PSF}$, and m are given in Eqs. (23), (24), and (25) and

$$\begin{aligned} \beta^{-1} &= m^2 + \frac{W_{\rm PSF}^2}{W_{\rm FOV}^2} \\ &= 1 + \frac{\alpha(\Delta - z)^2}{k^2}\left(a_0^2 + \frac{\Delta^2}{4k^2\rho_c^2}\right)^{-1}. \end{aligned} \tag{31}$$

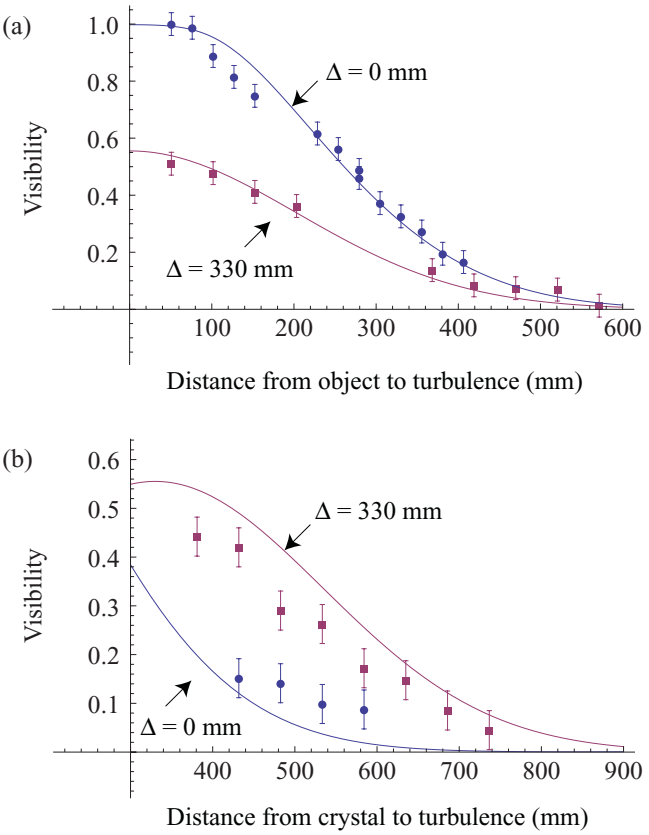

FIG. 4. (Color online) Plots of the visibilities when the turbulence layer is placed (a) between the object and the lens and (b) between the nonlinear crystal and the lens. The solid curves are theoretical plots from Eq. (29) with $\lambda = 2\pi/k = 0.65$ μm, $a_0 = 0.362$ mm, $\rho_c = 0.019$ mm, $d = 0.124$ mm, and $\alpha = 3.5$ mm^{-2}.

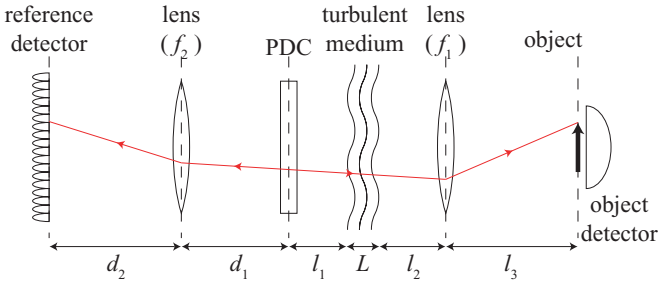

FIG. 5. (Color online) The Klyshko picture for the extended version of the model with a turbulent layer of finite thickness L.

It is remarked that since β is a function of α, the field of view depends on the strength of the turbulence when the turbulent layer is in the reference arm. The correlation factor in this case also changes with α as well as the locations of the turbulent layer and the down-conversion crystal. These features are all absent when the turbulent layer is in the object arm. In the limit when $\rho_c \to 0$, i.e., perfect correlation or anticorrelation in the biphoton transverse positions, $\beta \to 1$ and Eq. (30) becomes identical to Eq. (22).

V. EXTENSION TO TURBULENT LAYERS OF FINITE THICKNESS

We now wish to extend the model of Sec. III by allowing the turbulent layer to have an arbitrary finite thickness L. The generic setup of Fig. 1 now looks as shown in Fig. 5.

The calculation, though more cumbersome now, follows essentially the same pattern as in Secs. II and III, except that in place of Eq. (15) we use Eq. (12), which (maintaining the quadratic approximation) we now write in the form

$$\begin{aligned}&\langle h_{\rm turb}(\vec{\eta}_o,\vec{\xi}_o)h^*_{\rm turb}(\vec{\eta}'_o,\vec{\xi}'_o)\rangle\\&= \frac{k^2}{(2\pi)^2L^2}\exp\left(\frac{ik}{2L}|\vec{\eta}_o-\vec{\xi}_o|^2-\frac{ik}{2L}|\vec{\eta}'_o-\vec{\xi}'_o|^2\right)\\&\times\exp\left\{-\frac{\alpha}{6}[|\vec{\xi}_o-\vec{\xi}'_o|^2+(\vec{\xi}_o-\vec{\xi}'_o)\cdot(\vec{\eta}_o-\vec{\eta}'_o)\right.\\&\left.+|\vec{\eta}_o-\vec{\eta}'_o|^2]\right\},\end{aligned}\tag{32}$$

with $\alpha = 3/\rho_0^2$, as before. As a consequence, Eq. (17) now takes the form

$$\begin{aligned}&\langle H_o(\vec{x}_o,\vec{x}_s)H^*_o(\vec{x}'_o,\vec{x}'_s)\rangle\\&=\left(\frac{k}{2\pi L'}\right)^2\exp\left[\frac{ik}{2l}\left(1-\frac{l_2}{f_1}-\frac{L_1}{L'}\right)(|\vec{x}_o|^2-|\vec{x}'_o|^2)\right]\\&\times\exp\left[\frac{ik}{2L_1}\left(1-\frac{l}{L'}\right)(|\vec{x}_s|^2-|\vec{x}'_s|^2)\right]\\&\times\exp\left[-\frac{ik}{L'}(\vec{x}_o\cdot\vec{x}_s-\vec{x}'_o\cdot\vec{x}'_s)\right]\\&\times\exp\left[\frac{\alpha}{6}\frac{L''l^2L_1^2}{L^3l_1^2}|\vec{x}_o-\vec{x}'_o|^2\right]\exp\left[-\frac{\alpha}{6}\frac{L}{L_1}\Lambda|\vec{x}_s-\vec{x}'_s|^2\right]\\&\times\exp\left[\frac{\alpha}{3}\Lambda'(\vec{x}_s-\vec{x}'_s)\cdot(\vec{x}_o-\vec{x}'_o)\right],\end{aligned}\tag{33}$$

where l and l' are defined as previously, but we have made the new definitions

$$\frac{1}{L_0}=\frac{1}{L}+\frac{1}{l_1},\tag{34}$$

$$L_1 = L + l_1,\tag{35}$$

$$L' = L_1 + l - \frac{l_3L_1}{f_1},\tag{36}$$

$$L'' = L\left(1+\frac{L_0}{L}+\frac{L_0^2}{L^2}\right),\tag{37}$$

$$\Lambda = 1-\frac{l^2L_1^2}{L'^2L^3}\left[L''+\frac{L'L^2}{L_1l}\left(1+\frac{2l_1}{L_1}\right)\right],\tag{38}$$

$$\Lambda' = \frac{l^2L_1L''}{l_1L'^2L}-\frac{L}{L'}\left(1+\frac{2l_1}{L_1}\right).\tag{39}$$

Note that when we return to the previous thin-layer limit, $L \to 0$, these new parameters satisfy $\frac{L_0}{L} \to 1$, $L_1 \to l_1$, $L' \to l'$, and $\frac{L''}{L} \to 3$. Instead of Eq. (19), the second-order coherence function is now given by

$$\begin{aligned}&G^{(2)}(\vec{x}_o,\vec{x}_r)\\&=\left(\frac{k^2L_0L_1}{4\pi^2\delta l_1LL'}\right)^2\frac{AB}{\pi^2}\int d\vec{x}_i\,d\vec{x}_s\,d\vec{x}'_i\,d\vec{x}'_s\\&\times\exp\left\{-\vec{x}_s^2\left[\frac{\alpha}{6}\left(\frac{L_0}{l_1}\right)^2\Lambda-\frac{ik}{2L_1}\left(1-\frac{l}{L_1}\right)\right]\right\}\\&\times\exp\left\{-\vec{x}_s'^2\left[\frac{\alpha}{6}\left(\frac{L_0}{l_1}\right)^2\Lambda+\frac{ik}{2L_1}\left(1-\frac{l}{L_1}\right)\right]\right\}\\&\times\exp\left[\frac{ikL_0L_1}{L'Ll_1}\vec{x}_o\cdot(\vec{x}'_s-\vec{x}_s)\right]\\&\times\exp\left[\frac{\alpha}{3}\left(\frac{L_0}{l_1}\right)^2\Lambda\vec{x}_s\cdot\vec{x}'_s\right]\\&\times\exp\left[-\frac{ik}{2\delta f_2}d_2\left(|\vec{x}_i|^2-|\vec{x}'_i|^2\right)\right]\\&\times\exp\left\{\frac{ik}{2\delta}[|\vec{x}_i|^2-|\vec{x}'_i|^2-2\vec{x}_r\cdot(\vec{x}_i-\vec{x}'_i)]\right\}\\&\times\exp\left[-\frac{A+B}{4}\left(|\vec{x}_s|^2+|\vec{x}'_s|^2+|\vec{x}_i|^2+|\vec{x}'_i|^2\right)\right]\\&\times\exp\left[-\frac{A-B}{2}(\vec{x}_s\cdot\vec{x}_i+\vec{x}'_s\cdot\vec{x}'_i)\right].\end{aligned}\tag{40}$$

Once again, we specialize to the case of configuration 1; the expressions for configurations 2–4 may be found from the results by making the changes discussed in Sec. IV. Substituting the values given in Eq. (18), we find that

$$L_0 = \frac{Lz}{L+z},\tag{41}$$

$$L_1 = L+z,\tag{42}$$

$$L' = -\Delta,\tag{43}$$

$$L'' = L\left[1+\frac{z}{L+z}+\left(\frac{z}{L+z}\right)^2\right]\equiv L\eta,\tag{44}$$

$$\Lambda = 1 - \frac{(L+z)^2(z-\Delta+L)^2\eta}{\Delta^2 L^2} - \frac{z-\Delta+L}{\Delta L}\left(\frac{L+3z}{L+z}\right), \tag{45}$$

$$1 - \frac{l}{L'} = \frac{z+L}{\Delta}. \tag{46}$$

Notice that $\Lambda L^2 \to -3[\frac{z(z-\Delta)}{\Delta}]^2$ as $L \to 0$. First carrying out the $\vec{x}_i$ and $\vec{x}_i'$ integrals, we find

$$\begin{aligned} G^{(2)}(\vec{x}_o,\vec{x}_r) &= AB\left(\frac{k^2}{4\pi^2\Delta^2|\gamma|^2}\right)^2 \exp\left(-\frac{\vec{x}_r^2}{W'^2}\right)\int d\vec{x}_s\, d\vec{x}_s' \\ &\times \exp\left\{-\vec{x}_s^2\left[\left(\frac{1}{L+z}\right)^2\left(\frac{\alpha}{6}L^2\Lambda - \frac{ik}{2}\frac{(L+z)^2}{\Delta}\right) - \frac{A+B}{4} + \frac{(A-B)^2}{16\gamma}\right]\right\} \\ &\times \exp\left\{-\vec{x}_s'^2\left[\left(\frac{1}{L+z}\right)^2\left(\frac{\alpha}{6}L^2\Lambda + \frac{ik}{2}\frac{(L+z)^2}{\Delta}\right) - \frac{A+B}{4} + \frac{(A-B)^2}{16\gamma}\right]\right\} \\ &\times \exp\left[\frac{\alpha}{3}\left(\frac{L}{L+z}\right)^2\Lambda\vec{x}_s\cdot\vec{x}_s'\right] \\ &\times \exp\left[\vec{x}_s\cdot\left(\frac{ik}{\Delta}\vec{x}_o + \frac{ik(A-B)}{4\Delta\gamma}\vec{x}_r\right)\right] \\ &\times \exp\left[-\vec{x}_s'\cdot\left(\frac{ik}{\Delta}\vec{x}_o + \frac{ik(A-B)}{4\Delta\gamma}\vec{x}_r\right)\right], \end{aligned} \tag{47}$$

where

$$\gamma \equiv \frac{1}{4\rho_c^2} + \frac{ik}{2\Delta} \tag{48}$$

and

$$W'^2 \equiv \frac{4\Delta^2}{k^2}\left(\frac{1}{\gamma} + \frac{1}{\gamma^*}\right)^{-1} = \frac{\Delta^2}{4\rho_c^2 k^2} + \rho_c^2. \tag{49}$$

Finally, carrying out the $\vec{x}_s$ and $\vec{x}_s'$ integrations and making use of Eq. (1), we end up with a result for the ghost image that has the same form as Eq. (22),

$$P(\vec{x}_r) = \frac{1}{[2\pi W_{\rm FOV} W_{\rm PSF}(L)]^2}\exp\left(-\frac{|\vec{x}_r|^2}{2W_{\rm FOV}^2}\right) \times \int d\vec{x}_o\, |T(\vec{x}_o)|^2 \exp\left[-\frac{|\vec{x}_o + m\vec{x}_r|^2}{2W_{\rm PSF}^2(L)}\right], \tag{50}$$

except that $W_{\rm PSF}$ of Eq. (24) is replaced by

$$W_{\rm PSF}(L) = \left[\left(\rho_c^2 + \frac{\Delta^2}{4k^2a_0^2}\right) - \frac{\alpha\Delta^2}{3k^2}\left(\frac{L}{L+z}\right)^2\Lambda\right]^{1/2}. \tag{51}$$

Note that, though $W_{\rm PSF}(L)$ is a complicated function of L, it has identical dependence on the turbulence parameter α to $W_{\rm PSF}(0)$. The thickness L only alters the effective value of α.

It is straightforward to see that $W_{\rm PSF}(L) \to W_{\rm PSF}$ as $L \to 0$. At the other extreme, for $L \gg \max\{z,\Delta\}$, we find that $W_{\rm PSF}^2(L)$ increases quadratically with the thickness of the turbulent layer,

$$W_{\rm PSF}(L) \approx \left\{\rho_c^2 + \frac{\Delta^2}{4k^2a_0^2} + \frac{\alpha\Delta^2}{3k^2}\left[\left(\frac{L}{\Delta}\right)^2 - 1\right]\right\}^{1/2}, \tag{52}$$

reaching a maximum value of

$$W_{\rm PSF}(L_{max}) \approx \left[\rho_c^2 + \frac{\Delta^2}{4k^2a_0^2} + \frac{4\alpha f^2}{3k^2}\right]^{1/2} \tag{53}$$

when L reaches its maximum value of $L_{\rm max} = 2f + \Delta \approx 2f$. Further note that the field of view is still given by Eq. (23) and remains independent of the turbulence strength α.

VI. SUMMARY

In this paper, a detailed analysis of the quantum GI experiment in the presence of a turbulent medium is performed. It is shown that ghost images can be obtained with the turbulent medium located in either the object arm or the reference arm, while the characteristics of the ghost images differ slightly. Analytical expressions of the resolution and visibility under the quadratic structure function and Gaussian wave function approximations are obtained. The results show that, under the phase screen model of turbulence, the turbulent effect can be minimized by bringing the turbulent medium into the object plane. The results are consistent with the experiments and analysis in Ref. [11].

We have also extended the theory by allowing the turbulent layer to have arbitrary thickness L. Under the same quadratic approximations to the turbulence mutual coherence function and the quantum state of the entangled photon as those for the phase screen model, it is found that the results of the two cases differ only in the form of the width of the point spread function $W_{\rm PSF}$, which now depends on L in a complicated way. As expected, the two results converge when $L \to 0$. Though oversimplified, the phase screen model nevertheless gives good agreement with the experiment as well as a clear explanation of how the turbulent effect is minimized in the GI system.

Finally, it is remarked that the biphoton analysis reported here can be reproduced by a Gaussian-state treatment [17,18], which allows pseudothermal and SPDC ghost imagers to be treated on a common footing. In addition, this approach shows that there is a classical phase-sensitive configuration for GI that mimics almost all of the features seen in the quantum case.

ACKNOWLEDGMENTS

This research is supported by DARPA DSO InPho Grant No. W911NF-10-1-0404 and USARO MURI Grant No. W911NF-05-1-0197.

[1] D. N. Klyshko, Sov. Phys. Usp. **31**, 74 (1988).
[2] A. V. Belinskii and D. N. Klyshko, Sov. Phys. JETP **78**, 259 (1994).
[3] D. V. Strekalov, A. V. Sergienko, D. N. Klyshko, and Y. H. Shih, Phys. Rev. Lett. **74**, 3600 (1995).

[4] T. B. Pittman, Y. H. Shih, D. V. Strekalov, and A. V. Sergienko, Phys. Rev. A **52**, R3429 (1995).
[5] A. Gatti, E. Brambilla, M. Bache, and L. A. Lugiato, Phys. Rev. Lett. **93**, 093602 (2004).
[6] A. Valencia, G. Scarcelli, M. D'Angelo, and Y. Shih, Phys. Rev. Lett. **94**, 063601 (2005).
[7] J. Cheng, Opt. Express **17**, 7916 (2009).
[8] C. Li, T. Wang, J. Pu, and R. Rao, Appl. Phys. B **99**, 599 (2010).
[9] P. Zhang, W. Gong, X. Shen, and S. Han, Phys. Rev. A **82**, 033817 (2010).
[10] R. E. Meyers, K. S. Deacon, and Y. Shih, Appl. Phys. Lett. **98**, 111115 (2011).
[11] P. B. Dixon *et al*., Phys. Rev. A **83**, 051803 (2011).
[12] A. Ishimaru, *Wave Propagation and Scattering in Random Media* (Wiley-IEEE Press, New York, 1999).
[13] S. C. H. Wang and M. A. Plonus, J. Opt. Soc. Am. **69**, 1297 (1979).
[14] M. V. Fedorov, M. A. Efremov, P. A. Volkov, E. V. Moreva, S. S. Straupe, and S. P. Kulik, Phys. Rev. Lett. **99**, 063901 (2007).
[15] C. K. Law and J. H. Eberly, Phys. Rev. Lett. **92**, 127903 (2004).
[16] K. W. Chan, A. Jha, M. N. O'Sullivan-Hale, R. W. Boyd, and G. A. Tyler, CLEO/QELS 2007, Paper QWF2.
[17] B. I. Erkmen and J. H. Shapiro, Phys. Rev. A **77**, 043809 (2008).
[18] Nicholas D. Hardy, master of science thesis, MIT, 2011.